



HAL
open science

Controlled growth of Ni nanocrystals on SrTiO₃ and their application in the catalytic synthesis of carbon nanotubes

Jingyu R Sun, Chen R Wu, Fabien R Silly, Antal R Koós, Frank R Dillon,
Nicole R Grobert, Martin Castell

► **To cite this version:**

Jingyu R Sun, Chen R Wu, Fabien R Silly, Antal R Koós, Frank R Dillon, et al.. Controlled growth of Ni nanocrystals on SrTiO₃ and their application in the catalytic synthesis of carbon nanotubes. Chemical Communications, 2013, 49, pp.3748 - 3750. 10.1039/c3cc39114k . cea-01481329

HAL Id: cea-01481329

<https://cea.hal.science/cea-01481329>

Submitted on 2 Mar 2017

HAL is a multi-disciplinary open access archive for the deposit and dissemination of scientific research documents, whether they are published or not. The documents may come from teaching and research institutions in France or abroad, or from public or private research centers.

L'archive ouverte pluridisciplinaire **HAL**, est destinée au dépôt et à la diffusion de documents scientifiques de niveau recherche, publiés ou non, émanant des établissements d'enseignement et de recherche français ou étrangers, des laboratoires publics ou privés.

Controlled growth of Ni nanocrystals on SrTiO₃ and their application in the catalytic synthesis of carbon nanotubes†

Cite this: *Chem. Commun.*, 2013, **49**, 3748

Received 20th December 2012,
Accepted 18th March 2013

DOI: 10.1039/c3cc39114k

www.rsc.org/chemcomm

Jingyu Sun,^a Chen Wu,^a Fabien Silly,^b Antal A. Koós,^a Frank Dillon,^a Nicole Grobert^a and Martin R. Castell^{*a}

Truncated pyramid-shaped Ni nanocrystals were epitaxially grown on SrTiO₃(001) surfaces and characterised by scanning tunneling microscopy (STM). These nanocrystals were shown to be catalytically active for the synthesis of carbon nanotubes (CNTs). The narrow size distribution of the Ni nanocrystals results in a similar narrow distribution of CNT diameters.

Oxide supported metal nanocrystals are in widespread use in catalysis, microelectronics, gas sensing and optical applications.^{1–5} The morphologies of the nanocrystals can strongly affect their physical and chemical properties. For example, in the field of heterogeneous catalysis, it has been shown that tuning the sizes of oxide supported Au nanoparticles has a significant influence on their catalytic activity for CO oxidation.^{6,7} Extensive studies have also been undertaken on the fabrication of metal nanocrystals on oxide substrates for the preparation of CNT growth catalysts.^{8,9} A number of substrate materials have been explored (*e.g.* SiO₂, Al₂O₃, MgO) in combination with a variety of nanocrystal fabrication routes (wet chemistry, evaporation). However, it is still problematic to create oxide supported metal catalyst particles in a controllable manner with respect to uniformity of size and shape.^{10,11}

A strategy to circumvent this difficulty is to synthesise CNT catalyst particles on SrTiO₃ (STO)(001) single crystal surfaces. STO with its cubic perovskite structure, has been shown to allow the growth of metal nanocrystals with uniform size and shape distributions over macroscopic length scales.^{12–15} Moreover, due to the photocatalytic¹⁶ and dielectric¹⁷ properties of STO it may be possible to explore the nature of the resulting CNT–STO system in other novel scientific contexts. In this communication we report the use of an ultra-high vacuum (UHV) STM to study the growth of Ni nanocrystals on an atomically flat $c(4 \times 2)$

reconstructed STO(001) surface. We investigate the nucleation and Ostwald ripening of the nanocrystals, and determine their equilibrium shape and adhesion energy. The Ni/STO samples are then used in the catalytic synthesis of CNTs.

The substrate samples used in this study are 0.5 wt% Nb-doped STO(001) single crystals, supplied by PI-KEM Ltd, UK. After introducing the substrates into a JEOL JSTM-4500xt system operating at 10^{–8} Pa, they were outgassed through resistive heating. $c(4 \times 2)$ reconstructed surfaces were obtained by Ar⁺ ion sputtering, normally at 0.75 keV for 10 min, followed by a 1000 °C anneal in UHV for 1 h. Ni was deposited onto the $c(4 \times 2)$ reconstructed substrates from an e-beam evaporator (Oxford Applied Research EGN4) using 99.95% pure Ni rods supplied by Goodfellow Ltd, UK. For the STM studies, etched W tips were used for imaging the samples at either room temperature or elevated temperature (at 350 °C) with a bias voltage applied to the sample. To employ the STO supported Ni nanocrystals as catalysts for CNT growth, the sample was taken out of the UHV chamber and transferred into an atmospheric chemical vapour deposition (CVD) system, where ethanol-CVD (EtOH-CVD) was performed at a variety of growth temperatures. Details on the growth of CNTs can be found in the ESI.†

The substrate for Ni nanocrystal growth, the $c(4 \times 2)$ reconstructed STO(001) surface, was created in the UHV chamber and characterised by STM. A large scale image of the terraces on a $c(4 \times 2)$ surface, which has been well studied,^{18,19} is shown in the STM image in Fig. 1a. This surface features straight terrace edges that run along the [100] and [010] directions and also displays some isolated linear titanate nanostructures.^{20–22} Ni (2 monolayer (ML)) was deposited onto the room-temperature $c(4 \times 2)$ surface and subsequently annealed at 390 °C for 15 min. The Ni nanocrystals that form appear as bright spots with a square footprint in the STM image (Fig. 1b). The particles are randomly distributed without preferential nucleation along the terrace edges.

The sample was subject to further annealing at 320 °C for 13 h. This treatment induces Ostwald ripening of the nanocrystals and allows them to attain their equilibrium shape, as shown in the STM image in Fig. 2a, where the number of

^a Department of Materials, University of Oxford, Parks Road, Oxford OX1 3PH, UK.
E-mail: martin.castell@materials.ox.ac.uk

^b CEA, IRAMIS, SPCSI, Hybrid Magnetic Nanoarchitectures, F-91191 Gif-sur-Yvette, France

† Electronic supplementary information (ESI) available: Experimental details and product characterisations, hot-STM studies of ripening of Ni nanocrystals, further CNT growth experiments analysed by SEM, TEM, EDX, and Raman spectroscopy. See DOI: 10.1039/c3cc39114k

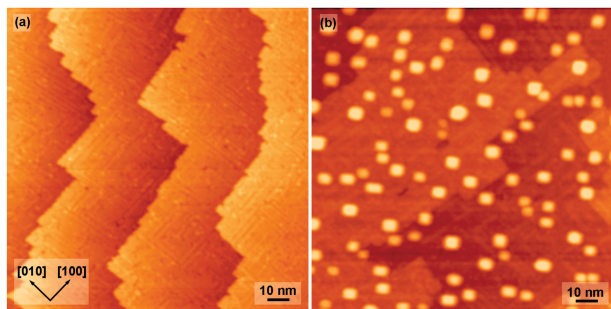


Fig. 1 STM images of the substrate before and after Ni nanocrystal growth. (a) The $c(4 \times 2)$ reconstructed $\text{SrTiO}_3(001)$ surface ($V_s = +1.5$ V, $I_t = 0.1$ nA). (b) Ni nanocrystals on the $c(4 \times 2)$ surface ($V_s = +1.0$ V, $I_t = 0.4$ nA).

nanocrystals has decreased but the average size has increased compared to Fig. 1b. The arrow in Fig. 2a denotes the line profile shown in Fig. 2b, which indicates the height and shape of the measured nanocrystal. The shape of the Ni nanocrystals is that of a truncated pyramid with its base edges parallel to the $\text{STO}(110)$ directions. Only this shape and epitaxial orientation was observed. Detailed image analysis indicates that the nanocrystal heights are quantised into steps of ~ 1.72 Å, which is consistent with the (001) lattice spacing for the fcc structure of Ni (1.76 Å). The side facets were measured to be at an angle of $53.1^\circ \pm 3.3^\circ$ to the surface, indicating (111) facets. These data indicate cube on cube epitaxy of $\text{STO}(001)||\text{Ni}(001)$, $\text{STO}(100)||\text{Ni}(100)$, as was also observed for Co,¹² Pd,²³ Cu,¹⁵ Pt,²⁴ and Ir²⁵ on $\text{STO}(001)$. The unit cell of STO is 3.905 Å, and that of Ni is 3.52 Å, which results in a tensile lattice mismatch of 9.86%. This epitaxial arrangement is therefore not possible without the introduction of misfit dislocations at the metal-oxide interface.

The ratio of the length (l) of the top square to the height (h) of the truncated pyramids (indicated in Fig. 2b) was determined over a range of volumes from 3 to 30 nm^3 . The l/h ratio does not change significantly with volume and is 1.18 ± 0.09 , implying that the nanocrystals have reached their equilibrium shape. A model of a nanocrystal (Fig. 2c) shows the equilibrium shape with a (001) top facet and four (111) side facets.

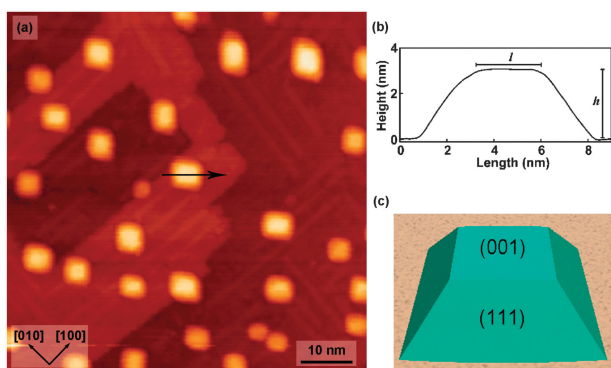


Fig. 2 (a) STM image of truncated pyramid shaped Ni nanocrystals on a $c(4 \times 2)$ surface after prolonged annealing ($V_s = +1.0$ V, $I_t = 0.4$ nA). (b) A line profile taken through a typical pyramid. The measured parameters l and h are indicated. (c) A 3D model of an fcc truncated pyramid shaped Ni nanocrystal.

The equilibrium shape of a supported Ni crystal depends on the surface energies of the Ni crystal facets (in this case, γ_{001} and γ_{111}), the surface energy of the substrate (γ_{STO}), and the interfacial energy between the Ni and the SrTiO_3 (γ_i). The change of the total energy of the Ni- SrTiO_3 system related to surfaces and interfaces is: $E = \gamma_{001}S_{001} + \gamma_{001}S_{111} + \gamma^*S_i$, where S_{001} and S_{111} are the Ni facet areas, S_i is the interfacial area, and γ^* is defined as $\gamma_i - \gamma_{\text{STO}}$. For a given nanocrystal volume, the equilibrium crystal shape is governed by the minimisation of the energy E . Using an analytical approach or the Winterbottom²⁶ analysis (also known as the Wulff-Kaischew theorem²⁷) for a truncated pyramid shaped particle equilibrated on a substrate leads to eqn (1).

$$\gamma^* = \sqrt{2} \frac{h}{l} (\sqrt{3} \gamma_{111} - \gamma_{001}) - \gamma_{001} \quad (1)$$

In this equation, the h/l value can be obtained from our experimental results, and the γ_{001} and γ_{111} values for fcc Ni are 2.77 J m^{-2} and 2.69 J m^{-2} , respectively,²⁸ which results in $\gamma^* = (-0.51 \pm 0.17) \text{ J m}^{-2}$. The adhesion energy, E_{ad} , of the Ni nanocrystal on the STO substrate, can be calculated according to eqn (2):

$$E_{\text{ad}} = \gamma_{001} + \gamma_{\text{STO}} - \gamma_i = \gamma_{001} - \gamma^* \quad (2)$$

This gives rise to $E_{\text{ad}} = (3.28 \pm 0.17) \text{ J m}^{-2}$.

An increased deposition amount of Ni to 4 ML leads to an increased Ni nanocrystal density on the STO substrate, without affecting the truncated pyramid shape formation, as shown in Fig. 3a. This STM image displays the topography of the surface following room-temperature deposition of 4 ML Ni and a subsequent 1 h anneal at 390°C . The areal density of the Ni particles is $(6.16 \pm 0.63) \times 10^{11} \text{ cm}^{-2}$, with a relatively uniform size distribution ranging mainly between 9–11 nm as shown in Fig. 3b. Moreover, the Ostwald ripening behaviour of the Ni nanocrystals has been investigated as a function of annealing time, where elevated-temperature STM (at 350°C) was performed, as shown in the ESI† (Fig. S1).

This study demonstrates controllable fabrication of Ni nanocrystals on $\text{STO}(001)$ with uniform size distribution and stable shape formation. In the next part of the paper we show how these Ni particles can be used for the catalytic synthesis of CNTs. Our CNT growth experiments were carried out by

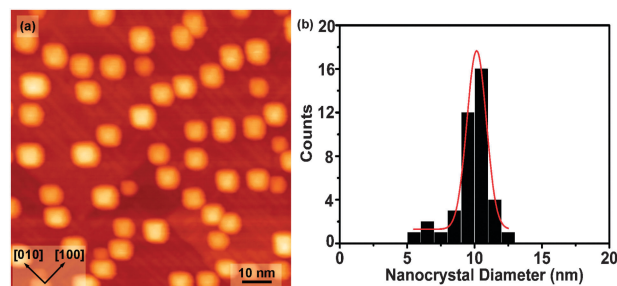


Fig. 3 Growth of truncated pyramid shaped supported Ni nanocrystals with high areal density and uniform size distribution. (a) STM image of Ni nanocrystals on a $\text{SrTiO}_3-c(4 \times 2)$ surface following 4 ML Ni deposition ($V_s = +1.0$ V, $I_t = 0.3$ nA). (b) The size distribution of grown Ni nanocrystals. Here the width of the square base of the Ni particles is measured.

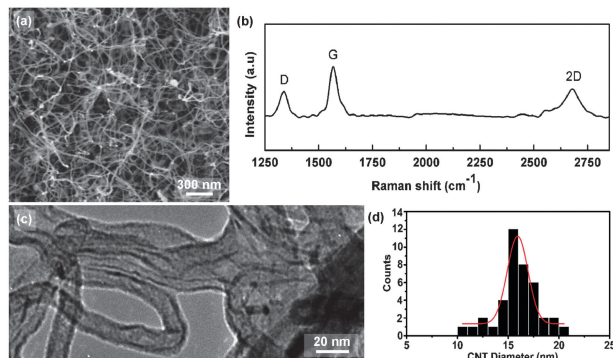


Fig. 4 Growth of CNTs on SrTiO₃(001) substrates using supported Ni nanocrystals as catalysts. (a–c) SEM image (a), Raman spectrum (b) and TEM micrograph (c) of CNTs. (d) The diameter distribution of the nanotubes.

atmospheric EtOH-CVD at a growth temperature of 800 °C, using a (400 : 200 sccm) mixture of Ar and H₂ flow. A typical scanning electron microscope (SEM) image (Fig. 4a) shows dense tubular structures covering the STO surface after the CVD process. The corresponding Raman spectrum (Fig. 4b) confirms that the nanostructures are CNTs with good quality (G/D ratio ~2 and a notable 2D peak indicating good crystallinity of CNTs). A transmission electron microscope (TEM) micrograph (Fig. 4c) shows that the nanotubes possess inner channels and are free of catalyst particles, however, the CNTs appear to be coated with a-C, which may be due to severe pyrolysis of feedstocks at CVD reactions at 800 °C. The diameter distribution of CNTs is shown in Fig. 4d. These results demonstrate that controlled synthesis of CNTs with tailored nanotube diameters can be achieved by using supported Ni nanocrystals with a homogeneous size distribution. We note that there is a difference between the nanocrystal sizes and nanotube diameters (Fig. 3b and 4d), which can be attributed to particle ripening that occurs at the growth temperature (800 °C) during the CNT synthesis process.

Further growth experiments have also been performed, showing that the Ni nanocrystals are catalytically active for synthesis of CNTs on STO substrates under various conditions (see ESI,† Fig. S2–S4). For example, low-temperature CNT synthesis at 600 °C was achieved, which is potentially desirable for applications in nanoelectronics; the use of different carbon precursors in the CVD process results in distinct carbon morphologies, indicating that the STO substrate is suitable to support the synthesis of carbon nanomaterials. Further optimisation of synthesis protocols aims to enhance the quality of the product (Fig. 4c) and ultimately achieve chirality-controlled growth of CNTs from the STO-supported metal particles. Our TEM observations also show that the CNTs are free of catalyst particles, thus indicating a base growth mode *i.e.* the Ni nanocrystal remains anchored to the substrate during CNT synthesis. The strong adhesion energy ($E_{ad} = 3.28 \text{ J m}^{-2}$) between the Ni particles and the STO support also indicates base mode growth. Previous studies have shown that with an E_{ad} value between 2.24 and 3.95 J m⁻² one would observe base mode growth of CNTs.²⁹ Our method for preparing metal catalysts could reduce the metal content of the produced

CNTs which eventually could make CNT purification processes unnecessary.

In summary, we have reported controllable synthesis of Ni nanocrystals on a SrTiO₃(001) support. The Ni nanocrystals adopt a truncated pyramid crystal shape with cube on cube epitaxy and an adhesion energy of $E_{ad} = (3.28 \pm 0.17) \text{ J m}^{-2}$. The supported Ni nanocrystals are used to catalyse CNT growth. This study offers insights into the use of the metal–SrTiO₃ system in tailored synthesis of CNTs, where several key issues are tackled: (1) difficulty in producing uniform size and shape distributions of the catalyst; (2) difficulty in efficient growth of CNTs on electrically conducting substrates, especially at low temperatures. SrTiO₃ becomes an n-type semiconductor after doping (*e.g.* with Nb or La), and this may be of technological importance, in particular for nanoelectronic device fabrication, as a common requirement is direct electrical contact between the CNTs and the substrate.³⁰

We are grateful to the Royal Society (NG), ERC Starting Grant (ERC-2009-StG 240500) (NG), and CME-UO joint Scholarship (JS) for financial support. We also thank Chris Spencer (JEOL, UK) for valuable technical support.

Notes and references

- 1 M. Batzill and U. Diebold, *Phys. Chem. Chem. Phys.*, 2007, **9**, 2307.
- 2 M. S. Chen and D. W. Goodman, *Science*, 2004, **306**, 252.
- 3 A. M. Doyle, S. K. Shaikhutdinov, S. D. Jackson and H. J. Freund, *Angew. Chem., Int. Ed.*, 2003, **42**, 5240.
- 4 Q. Fu and T. Wagner, *Surf. Sci. Rep.*, 2007, **62**, 431.
- 5 J. Y. Yang, J. H. Kim, W. J. Choi, Y. H. Do, C. O. Kim and J. P. Hong, *J. Appl. Phys.*, 2006, **100**, 066102.
- 6 J. L. Lu, H. J. Gao, S. Shaikhutdinov and H. J. Freund, *Catal. Lett.*, 2007, **114**, 8.
- 7 M. Valden, X. Lai and D. W. Goodman, *Science*, 1998, **281**, 1647.
- 8 P. B. Amama, C. L. Pint, S. M. Kim, L. McJilton, K. G. Eyink, E. A. Stach, R. H. Hauge and B. Maruyama, *ACS Nano*, 2010, **4**, 895.
- 9 S. Esconjauregui, M. Fouquet, B. C. Bayer, C. Ducati, R. Smajda, S. Hofmann and J. Robertson, *ACS Nano*, 2010, **4**, 7431.
- 10 M. Kumar and Y. Ando, *J. Nanosci. Nanotechnol.*, 2010, **10**, 3739.
- 11 J. P. Tessonnier and D. S. Su, *ChemSusChem*, 2011, **4**, 824.
- 12 F. Silly and M. R. Castell, *Appl. Phys. Lett.*, 2005, **87**, 053106.
- 13 F. Silly and M. R. Castell, *Appl. Phys. Lett.*, 2005, **87**, 063106.
- 14 F. Silly and M. R. Castell, *Phys. Rev. Lett.*, 2006, **96**, 086104.
- 15 F. Silly and M. R. Castell, *ACS Nano*, 2009, **3**, 901.
- 16 M. Miyachi, M. Takashio and H. Tobimatsu, *Langmuir*, 2004, **20**, 232.
- 17 J. H. Haeni, P. Irvin, W. Chang, R. Uecker, P. Reiche, Y. L. Li, S. Choudhury, W. Tian, M. E. Hawley, B. Craigo, A. K. Tagantsev, X. Q. Pan, S. K. Streiffer, L. Q. Chen, S. W. Kirchoefer, J. Levy and D. G. Schlom, *Nature*, 2004, **430**, 758.
- 18 M. R. Castell, *Surf. Sci.*, 2002, **505**, 1.
- 19 N. Erdman, O. Warschkow, M. Asta, K. R. Poepelmeier, D. E. Ellis and L. D. Marks, *J. Am. Chem. Soc.*, 2003, **125**, 10050.
- 20 M. R. Castell, *Surf. Sci.*, 2002, **516**, 33.
- 21 M. S. J. Marshall, A. E. Becerra-Toledo, L. D. Marks and M. R. Castell, *Phys. Rev. Lett.*, 2011, **107**, 086102.
- 22 D. S. Deak, K. Porfyraakis and M. R. Castell, *Chem. Commun.*, 2007, 2941.
- 23 F. Silly and M. R. Castell, *Phys. Rev. Lett.*, 2005, **94**, 046103.
- 24 H. Iddir, V. Komanicky, S. Ogut, Y. Hoydoo and P. Zapol, *J. Phys. Chem. C*, 2007, **111**, 14782.
- 25 B. Koslowski, R. Notz and P. Ziemann, *Surf. Sci.*, 2002, **496**, 153.
- 26 W. L. Winterbottom, *Acta Metall. Mater.*, 1967, **15**, 303.
- 27 R. Kaischew, *Bull. Bulg. Acad. Sci., Phys. Ser.*, 1950, **1**, 100.
- 28 M. Alden, S. Mirbt, H. L. Skriver, N. M. Rosengaard and B. Johansson, *Phys. Rev. B*, 1992, **46**, 6303.
- 29 Y. Wang, Z. Luo, B. Li, P. S. Ho, Z. Yao, L. Shi, E. N. Bryan and R. J. Nemanich, *J. Appl. Phys.*, 2007, **101**, 124310.
- 30 G. D. Nessim, M. Seita, K. P. O'Brien, A. J. Hart, R. K. Bonaparte, R. R. Mitchell and C. V. Thompson, *Nano Lett.*, 2009, **9**, 3398.